A Simplified Broadband Coupling Approach Applied to Chemically Robust Sol−Gel, Planar Integrated Optical Waveguides

John Thomas Bradshaw,[†] Sergio B. Mendes,[‡] and S. Scott Saavedra*,[†]

Department of Chemistry, University of Arizona, Tucson, Arizona 85721, and Optical Sciences Center, University of Arizona, Tucson, Arizona 85721

A new generation waveguide spectrometer with broadband coupling capabilities has been developed. As opposed to previous devices, this attenuated total reflection (ATR) spectrometer is much simpler in design, is more chemically robust, and transmits light down to at least 400 nm. The attenuated total reflection element consists of a single-mode, planar integrated optical waveguide fabricated by dip-coating a ∼300 nm thick, sol−gel composite layer on a glass substrate. A commercially available prism is used as the incoupler with an integral holographic diffraction grating acting as the dispersive outcoupling element. The transmission of narrow band-pass filters was used to compare the response of the waveguide spectrometer to that of a conventional transmission instrument. Spectral resolution was assessed by measuring the fwhm of various laser lines, which were found to range from 0.5 to 1.3 nm. The measured limits of detection for the waveguide spectrometer from 400 to 600 nm are 8.0 and 10.1 milliabsorbance units for TE and TM polarizations, respectively. Finally, to demonstrate the application of this technology to a molecular film confined to a solid−liquid interface, visible ATR spectra of an adsorbed submonolayer of horse heart cytochrome *c* were acquired. A procedure to correct the waveguide spectra for the wavelength dependence in ATR path length is described.

Planar and cylindrical waveguides have been used as spectroscopic tools for analyzing thin films and interfaces for many years.[1−8] Most of these waveguides have been relatively thick devices capable of supporting thousands of guided modes. Single-mode planar integrated optical waveguide (IOW) structures have been shown to be inherently more sensitive by a few orders of magnitude than their much thicker multimode counterparts.[9,10] This is primarily due to the ability of a single-mode IOW to support several thousand reflections per centimeter of beam propagation, which leads to an overall increase in the attenuated total reflection (ATR) path length and a corresponding sensitivity enhancement. This feature has been exploited in the development of various IOW tools, ranging from devices designed to characterize surfaces[11] and thin films[12−17] to chemical sensor platforms.[18−21]

Although single-mode planar IOWs are very useful tools for studying interfaces, they do suffer from one major disadvantage: narrow spectral bandwidth. This limitation is inherent because of the dependence of the internal reflection angle on the wavelength of propagating light.[22,23] More specifically, a phase shift occurs as light is totally reflected at the interfaces in a waveguide. The result is that only discrete internal reflection angles lead to harmonic solutions (modes) and allow for light propagation. For a single-mode IOW, this condition means that different wavelengths of light must propagate at different internal reflection angles to produce a guided mode for each wavelength. The practical consequence is that for a given experimental configuration (i.e., optical alignment), an ATR measurement can be performed at only a single wavelength, or at best over a very narrow spectral window, which limits the information content of the experiment.

* To whom correspondence should be addressed. Phone: (520) 621-9761. Fax: (520) 621-8407.

† Department of Chemistry.

‡ Optical Sciences Center.

(1) Seitz, W. R. *Anal. Chem.* **1984**, *56*, 17A−34A.

(2) Bohn, P. W. *Trends Anal. Chem.* **1987**, *6*, 223−233.

(3) Stephens, D. A.; Bohn, P. W. *Anal. Chem.* **1989**, *61*, 386−390.

(4) Dessy, R. E. *Anal. Chem.* **1989**, *61*, 1079A.

(5) Kang, L.; Dessy, R. E. *Crit. Rev. Anal. Chem.* **1990**, *21*, 377−388.

(6) Arnold, M. A. *Anal. Chem.* **1992**, *64*, 1015A−1025A.

(7) Qing, D.; Yamaguchi, I.; Itoh, K.; Murabayashi, M. *Opt. Rev.* **1997**, *4*, 578−583.

(8) Mogensen, K. B.; Friis, P.; Hubner, J.; Petersen, N.; Jorgensen, A. M.; Telleman, P.; Kutter, J. P. *Opt. Lett.* **2001**, *26*, 716−718.

(9) Saavedra, S. S.; Reichert, W. M. *Anal. Chem.* **1990**, *62*, 2251−2256.

(10) Mendes, S. B.; Saavedra, S. S. *Opt. Express* **1999**, *4*, 449−456.

(11) Horvath, R.; Voros, J.; Graf, R.; Fricsovszky, G.; Textor, M.; Lindvold, L. R.; Spencer, N. D.; Papp, E. *Appl. Phys. B* **2001**, *72*, 441−447.

(12) Plowman, T. E.; Garrison, M. D.; Walker, D. S.; Reichert, W. M. *Thin Solid Films* **1994**, *243*, 610−615.

(13) Lee, J. E.; Saavedra, S. S. In *Proteins at Interfaces II*; Horbett, T. A., Brash, J. L., Eds.; ACS Symposium Series 602; American Chemical Society: Washington, (D. C.), 1995; pp 269−279.

(14) Ball, V.; Ramsden, J. J. *J. Phys. Chem. B* **1997**, *101*, 5465−5469.

(15) Edmiston, P. L.; Saavedra, S. S. *Chem. Mater.* **1997**, *9*, 2599−2603.

(16) Edmiston, P. L.; Lee, J. E. *J. Am. Chem. Soc.* **1997**, *119*, 560−570.

(17) Edmiston, P. L.; Saavedra, S. S. *J. Am. Chem. Soc.* **1998**, *120*, 1665−1671.

(18) Yang, L.; Saavedra, S. S. *Anal. Chem.* **1995**, *67*, 1307−1314.

(19) Yang, L.; Saavedra, S. S.; Armstrong, N. R. *Anal. Chem.* **1996**, *68*, 1834−1841.

(20) Skrdla, P. J.; Saavedra, S. S.; Armstrong, N. R.; Mendes, S. B.; Peyghambarian, N. *Anal. Chem.* **1999**, *71*, 1332−1337.

(21) Voros, J.; Graf, R.; Kenausis, G. L.; Bruinink, A.; Mayer, J.; Textor, M.; Wintermantel, E.; Spencer, N. D. *Biosens. Bioelectron.* **2000**, *15*, 423−429.

(22) Kogelnik, H. In *Integrated Optics*; Tamir, T., Ed.; Springer-Verlag: New York, 1979; Vol. 7, pp 13−81.

(23) Plowman, T. E.; Saavedra, S. S.; Reichert, W. M. *Biomaterials* **1998**, *19*, 341−355.

Attempts to overcome the narrow spectral bandwidth of planar IOWs have been described.[24-29] The first truly successful solutions to broadband coupling were created and reported by Mendes et al.[30-32] The general approach consisted of theoretically designing and implementing an incoupling element that effectively dispersed a ~110 nm band of light, incident at a single launch angle, to yield bound waveguide modes for all wavelengths. Thus, every wavelength in this spectral window was achromatically coupled into and propagated in the waveguide layer with high efficiency. Two approaches were taken in designing broadband coupling elements. The first consisted of a multicomponent incoupler consisting of a single prism and two gratings.[30,31] In the second, the optical dispersion characteristics of the waveguiding layer were "tailored" to allow achromatic coupling using a single prism.[32] Both devices were used to construct a multichannel IOW spectrometer with which ATR spectra could be measured over a bandwidth of >100 nm. In both cases, a major disadvantage was the chemical ruggedness, or lack thereof, of the vacuum-deposited, Corning 7059 glass waveguiding layer. Attempts to clean these waveguides in oxidizing acids (Chromerge or piranha) resulted in etching of the Corning 7059 layer and consequent loss of its light-guiding capabilities. Furthermore, with optical losses of ~2 dB/cm, these waveguides were only marginally acceptable for measuring ATR spectra of weakly adsorbing samples.[33] Finally, the incoupling elements (vide supra) required custom fabrication and, in the case of the multicomponent incoupler, precise alignment in order to operate properly.

We report in this paper a much simpler broadband coupling approach that allows for the entire visible region of light to be guided at one incident angle. Broadband coupling into a chemically robust, sol-gel glass, single-mode planar IOW is achieved using a commercially available prism incoupler. Outcoupling occurs at an integral holographic grating, which spectrally disperses the entrapped light; thus, multichannel ATR spectra can be acquired without using a monochromator. The optical performance of this broadband IOW-ATR spectrometer is characterized and compared to that of a commercially available, transmission-based spectrometer. Finally, the utility of this device for measuring polarized ATR spectra of a thin molecular film of horse heart cytochrome *c* is demonstrated.

EXPERIMENTAL SECTION

Waveguide Fabrication. The basic waveguide structure, similar to previous designs,[18-20,34] consisted of two components:

(1) a substrate containing a holographic diffraction grating and (2) a sol-gel waveguide film deposited on the substrate. In brief, soda lime glass microscope slides (Gold Seal) were cleaned by manually scrubbing with cotton soaked in a 1% Liqui-Nox surfactant mixture (Alconox) and liberally rinsed with 18.1 MΩ/cm deionized water (Barnstead Nanopure). The slides were then immersed in a heated (60-80 °C) Chromerge (Manostat) bath for 20-30 min. Upon removal, the slides were liberally rinsed with Nanopure water, blown dry with a nitrogen stream, placed in a staining dish and dried in a 100 °C oven for at least 30 min. Once dry, the slides were not removed from the sealed dish until grating fabrication occurred (in order to avoid particulate adsorption).

Grating fabrication, previously reported by Li et al.,[35,36] was accomplished via a holographic microfabrication process. In brief, a ~200-nm-thick film of photoresist (Shipley 1805) was deposited onto a clean microscope slide. The grating pattern was then written into the photoresist using the 441.6 nm line of a He-Cd laser (TE$_{00}$, Kimmon) via a Lloyd's mirror arrangement, and developed by controlled immersion into developer solution (Shipley 351). The grating was then written into the microscope slide substrate (through the previously developed photoresist mask) by a reactive ion etching process using Freon as the reactive gas species. The remaining photoresist was then removed by vigorous scrubbing and successive sonication in acetone, ethanol/methanol, and finally, Liqui-Nox. The grating period was determined by measuring the diffraction angle in the Littrow configuration and confirmed by atomic force microscopy (AFM).

Prior to waveguide deposition, substrates containing gratings were subjected to Chromerge cleaning (vide supra) and thoroughly dried. Sol-gel waveguide films were deposited by dip-coating at a speed of 0.3 cm/sec in a controlled atmosphere of 25 °C and relative humidity of 10-20%. The sol-gel formulation that was used consisted of a 14:11.5:4.2:1 (v/v) mixture of ethanol (200 proof, AAPER Chemical), methyltriethoxysilane (99%, Aldrich), titanium (IV) butoxide (97%, Aldrich), and silicon tetrachloride (99.998%, Aldrich). Films were cured in a 500 °C tube furnace for 20 min in air. The resulting waveguide layers were 300-400 nm thick and displayed optical dispersion curves approximated by $n_w = 1.57 + 14,000/\lambda^2$ (i.e., the refractive index at 457.9 nm was ~1.64), as determined by measuring the incident coupling angle at multiple wavelengths.[37] Through this analysis, the waveguide layers were found to support only TE$_0$ and TM$_0$ modes for all wavelengths measured (ranging from 457.9 to 830 nm). Waveguide propagation loss was not determined but was assumed to be comparable to that of very similar sol-gel waveguides previously prepared and characterized in our lab (~0.2 dB/cm).[34]

Optical Layout. A truncated, right angle (45-45-90) Schott glass prism (SF6, Karl Lambrecht) was used as the incoupling element for all experiments (Figure 1a). The prism was mounted in a black plexiglass flow cell with black silicon adhesive, similar to that previously reported by Saavedra and Reichert.[38] After mounting the waveguide in the flow cell and ensuring that the gap between the base of the prism and the waveguide surface was filled with water (by filling the flow cell), pressure was applied

(24) Midwinter, J. E. *IEEE J. Quantum Electron.* **1971**, *QE-7*, 345-350.

(25) Spaulding, K. E.; Morris, G. M. *Appl. Opt.* **1991**, *30*, 1096-1112.

(26) Spaulding, K. E.; Morris, G. M. *J. Lightwave Technol.* **1992**, *10*, 1513-1518.

(27) Hetherington, D. L.; Kostuk, R. K.; Gupta, M. C. *Appl. Opt.* **1993**, *32*, 303-308.

(28) Strasser, T. A.; Gupta, M. C. *Appl. Opt.* **1994**, *33*, 3220-3226.

(29) Li, L.; Brazas, J. C. J.; U.S. Patent 5,420,947, May 30, 1995; p 12.

(30) Mendes, S. B.; Li, L.; Burke, J. J.; Lee, J. E.; Saavedra, S. S. *Appl. Opt.* **1995**, *34*, 6180-6186.

(31) Mendes, S. B.; Li, L.; Burke, J. J.; Lee, J. E.; Dunphy, D. R.; Saavedra, S. S. *Langmuir* **1996**, *12*, 3374-3376.

(32) Mendes, S. B.; Li, L.; Burke, J. J.; Saavedra, S. S. *Opt. Comm.* **1997**, *136*, 320-326.

(33) Chartier, G. In *Integrated Optics: Physics and Applications*; Martellucci, S., Chester, A. N., Eds.; Plenum Press: New York, 1981; Vol. 91, pp 49-72.

(34) Yang, L.; Saavedra, S. S.; Armstrong, N. R.; Hayes, J. *Anal. Chem.* **1994**, *66*, 1254-1263.

(35) Li, L.; Xu, M.; Stegeman, G. I.; Seaton, C. T. *Proc. SPIE-Int. Soc. Opt. Eng.* **1987**, *835*, 72-82.

(36) Brazas, J. C.; Li, L. *Appl. Opt.* **1995**, *34*, 3786-3792.

(37) Saavedra, S. S.; Reichert, W. M. *Appl. Spectrosc.* **1990**, *44*, 1210-1217.

(38) Saavedra, S. S.; Reichert, W. M. *Appl. Spectrosc.* **1990**, *44*, 1420-1423.
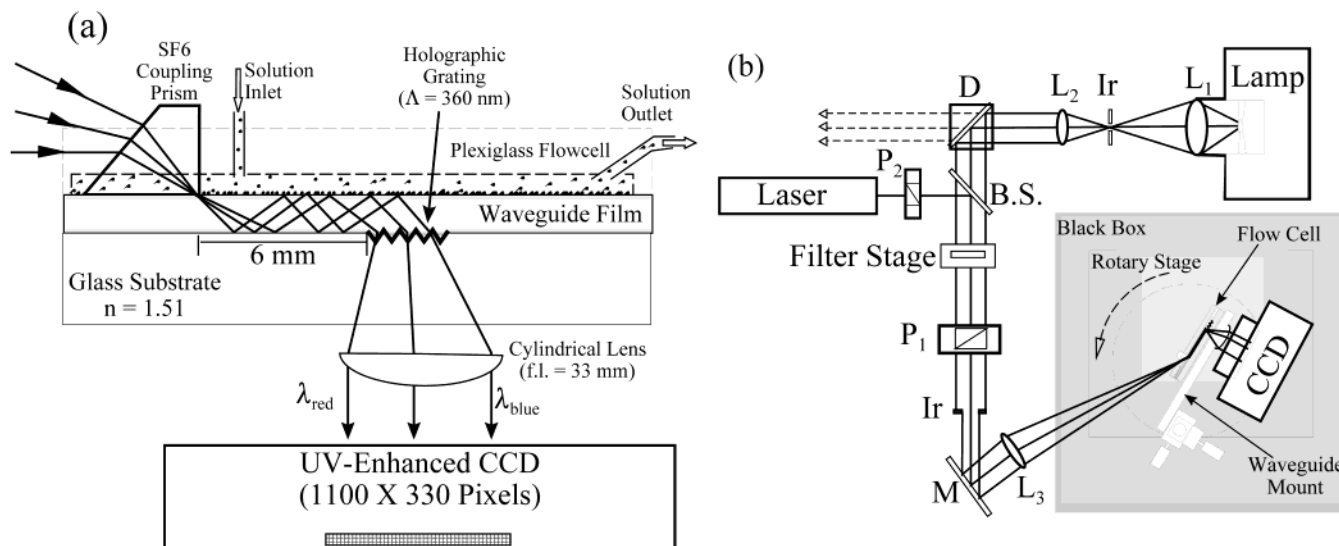
Figure 1. Optical layout of the broadband sol−gel planar IOW spectrometer. (a) Light is focused into the SF6 prism, coupled into the sol−gel waveguiding layer, and outcoupled through the glass substrate by a surface relief grating (grating period = 360 nm). The outcoupled light is collimated using a 33-mm-focal-length (f.l.) cylindrical lens onto a CCD camera. Incoupler-to-outcoupler distance for experiments reported herein ranged from 6 to 9 mm. (b) Optical beam path through components: L_1 = 48 cm f.l. lens, Ir = iris, L_2 = 8 cm f.l. lens, D = 470 nm dichroic long pass filter, B.S. = beam splitter, P_1 = Glan-Taylor UV prism polarizer, M = mirror, and L_3 = 43 cm f.l. lens. The B.S. and a second polarizer (P_2) were used to introduce various laser sources into the beam path and to adjust their intensities. A filter stage was used to place narrow band-pass filters in the beam path.

to the top of the prism via a mounting clamp to achieve coupling. Filling the prism−waveguide gap with solution is required to maintain a constant mode profile across the entire waveguide (i.e., from the incoupling prism to the outcoupling grating), as described previously.[37,38]

A 150 W xenon arc lamp (ORIEL) provided the white light output for all experiments (Figure 1b). An image of the arc was focused, spatially filtered, and then collimated. The beam was then reflected from a dichroic filter (DCLP 470, Omega Optical), passed through a Glan-Taylor UV prism polarizer (Karl Lambrecht) and an iris, reflected from a mirror, and focused onto the vertex of the waveguide coupling prism. The waveguide flow cell was mounted on an *XYZ* translational stage (Daedal) and on a precision rotary stage (0.001° resolution, New England Affiliated Technologies). The light outcoupled from the waveguide was collected using a 33-mm-focal-length cylindrical lens attached to the back of the waveguide mount. A TE-cooled CCD camera (Roper Scientific) was aligned and mounted to the rotary stage. To minimize stray light, the entire rotary stage was placed inside a light-tight enclosure.

Broadband Waveguide Spectrometer Characterization. All waveguide experiments were performed while the flow cell was filled with 50 mM, pH 7 sodium phosphate buffer. The broadband response of the waveguide was visually verified (vide infra) prior to any experimentation. Upon achieving broadband coupling, a 514-nm narrow band-pass laser line filter was inserted into the optical train (Figure 1b) and used to focus the CCD. Wavelength calibration was accomplished by measuring the peak throughput of various narrow band-pass filters. Various laser lines were used for wavelength calibration and assessing spectral resolution; they were aligned collinearly with the optical axis of the xenon lamp using a beam splitter (Figure 1b). Image exposure times were determined by measuring the CCD response to successively

longer integration times, with ∼80% of full well capacity used as the integration time for all experiments.

Protein Adsorption Protocol. Prior to any protein adsorption experiments, the sol−gel waveguides were cleaned in a heated Chromerge bath, rinsed with 18.1 MΩ water, soaked for ∼30 min in a 1 M HNO_3 solution to rehydrate the surface and rinsed again. With the waveguide mounted in the flow cell, raw throughput intensities for both TE and TM polarizations were measured as a function of angle (over ∼3° range centered about the initial coupling angle) in order to maximize throughput at 400 nm, which is the region in which the Soret band of horse heart cytochrome *c* occurs. Optimizing waveguide throughput in this region also required the use of the long pass dichroic filter (vide supra). The protein adsorption experiment was performed by first collecting a reference spectrum of 50 mM sodium phosphate buffer. Next, 50 μM horse heart ferricytochrome *c* (99%, Sigma), freshly purified by separation on a carboxymethyl cellulose column (CM-52, Whatman),[39] was injected into the flow cell and incubated at room temperature for 30 min. Previous experience has shown that this results in adsorption of about one monolayer on a glass IOW surface.[16] Because of the high molar absorptivity in the vicinity of the Soret band (vide infra), less than a monolayer of material was required in order to remain below the stray light limit in this spectral range. Thus, a portion of the adsorbed cytochrome *c* was desorbed from the waveguide surface by injection of 0.5 M phosphate buffer, and the spectral response was measured. The adsorbed ferricytochrome *c* was then reduced by injection of 8 mM sodium dithionite (J. T. Baker), and the spectrum of the adsorbed ferrocytochrome *c* film was collected. In the final step, the spectrum of the adsorbed protein film was collected after reoxidation by injection of 8 mM ferricyanide (99.96%, Mallinck-

(39) Brautigan, D. L.; Ferguson-Miller, S.; Margoliash, E. In *Methods in Enzymology*; Academic Press: New York, 1978; Vol. 53D, pp 128−164.
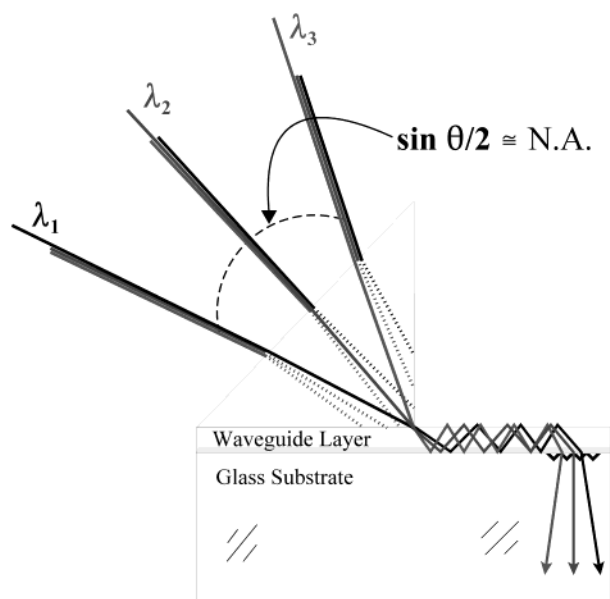
Figure 2. Schematic illustration of the simple broadband coupling approach. A relatively large N.A. beam is incident onto an incoupling prism. Within the incident cone, there exists angular coupling solutions for λ_1, λ_2, and λ_3. These wavelengths are effectively coupled into the waveguide layer at the appropriate incident angles that produce resonant modes, but are rejected at off-resonance angles. Thus, in principle, a portion of light from each wavelength should be coupled into the waveguide layer.

rodt). For each step, a spectrum was also collected after flushing the cell with buffer.

RESULTS AND DISCUSSION

Broadband Coupling Phenomenon. The second of the two achromatic couplers described by Mendes et al.[32] consisted of a single prism incoupler matched to a specific waveguide layer. This strategy appeared to be the more feasible for our purposes (mainly because of the difficulties associated with creating a multicomponent coupler)[30] and was pursued in an effort to create an IOW-ATR spectrometer using a sol−gel-derived, planar IOW. We sought to create a sol−gel waveguiding layer with optical dispersion properties similar to a commercially available glass. Specifically, the sol−gel formulation was iteratively altered to "tune" the waveguide optical dispersion to match a single prism incoupler. Multiple attempts did not produce a match. They instead produced IOWs for which no achromatic coupling solution could be achieved using a prism fabricated from commercially available glasses. Therefore, an alternative, much simpler strategy was explored.

In this approach, a relatively large numerical aperture (N.A.) beam was focused onto an incoupling prism. Figure 2 illustrates this approach wherein every wavelength in the incident beam is refracted at the prism surface at every angle within the incident cone. If the N.A. of the beam is large enough, there should exist an incoupling angle that corresponds to an incoupling solution for each wavelength within a broad spectral range. In other words, λ_1, λ_2, and λ_3 will simultaneously and effectively couple into the waveguide at incident angles that produce resonant modes but will be rejected at incident angles that do not correspond to coupling solutions. In contrast to the achromatic solutions
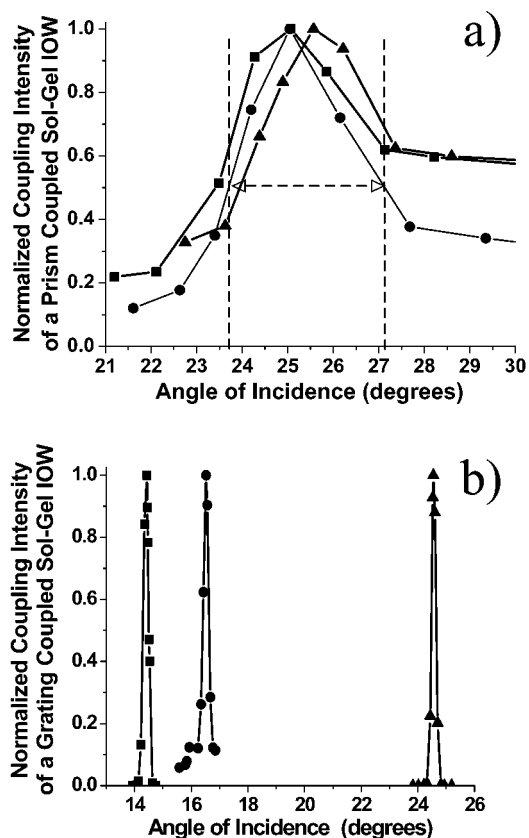
Figure 3. Normalized outcoupling intensity profiles for laser lines 514.5 nm (■), 496.5 nm (●), and 457.9 nm (▲) measured as a function of incident beam coupling angle for (a) a prism-coupled and (b) a grating-coupled sol−gel waveguide. Individual curves were normalized to their respective maximum intensity. The dashed lines in part a indicate the fwhm (~3.6°) of the 496.5-nm profile.

described above (wherein every wavelength in the spectral window is dispersed into the waveguide with high efficiency),[30−32] the principal issue with this simpler approach is how much energy can be coupled into the waveguide versus the amount that is discarded by off-angle incidence. As shown below, sufficient light couples into a single-mode sol−gel waveguide to make this a viable strategy for performing broadband IOW-ATR spectroscopy.

The first attempt to implement this approach consisted of incoupling the "all lines" mode of a 6 W argon ion laser (Coherent, I70−5) into a waveguide. The observed response was that all the Ar+ lines (457.9, 476.5, 488.0, 496.5, 501.7, and 514.5 nm) were effectively coupled at a single incident angle into the waveguiding layer, guided along its axis and outcoupled at the diffraction grating. Hence, a 56.6-nm bandwidth was observed to "guide" at one incident angle.

To determine the nature of the observed broadband coupling, the dependence of outcoupling intensity on the incident angle for several of the Ar+ laser lines was measured. Figure 3a clearly shows that the outcoupling intensity of three different laser lines is very broad (457.9, 496.5, and 514.5 nm). In comparison, Figure 3b shows the normalized coupling efficiency of a grating incoupler used on a sol−gel waveguide. Note the strong overlap of the prism coupling profiles (Figure 3a) versus the baseline resolution of the grating coupling profiles (Figure 3b). The fwhm of the 496.5-nm mode, represented by the dashed lines in Figure 3a, corresponds to an angular width of ~3.6°. This angular width can be achieved

using an incident beam with a N.A. of 0.03 (approximately the sine of the half angle). The data also show that at an incident angle of ~25.5°, all three laser lines are prism-incoupled at >90% of their maximum coupling efficiency as a result of the strong angular overlaps among the wavelengths.

Further analysis of the broadband coupling shown in Figure 3a required a comparison of the optical properties of the waveguide layer with those of the incoupling prism. Theoretical calculations based upon optical dispersion cancellation (see Mendes et al.[32]) showed that the prism coupler was not achromatically coupling the light into the waveguide. Thus, broadband coupling was achieved simply by a favorable match between the numerical aperture of the incident beam and the angular acceptance range inherent in the waveguide structure (i.e., the phenomenon depicted in Figure 2).

A white light source (xenon lamp) was used to determine the maximum bandwidth over which broadband coupling could be efficiently achieved. It is difficult to visually distinguish a waveguide streak from the zigzag path of a mode guided in the substrate when an incoherent source is used (because of a larger spot size; lower intensity for individual wavelengths; and poor collimation, as compared to a coherent laser source). Two approaches were used to ensure that the observed response using the xenon lamp was due to light propagation through the ~400 nm sol−gel layer (waveguide modes) and not through the entire microscope slide (substrate modes). First, laser lines were coupled into the waveguide simultaneously with the white light source. This was accomplished by collinear alignment of a 5.0 mW HeNe laser (543.4 nm), a 30 mW HeNe laser (632.8 nm), and a 6 W Ar+ laser (in the "all lines" mode) with the white light source. With proper alignment, the laser lines were visually observed to produce a waveguide streak, *and* the outcoupling angles for the laser lines and the white light were approximately equal, which provided evidence that white light waveguiding was occurring. The second method consisted of applying a small spot of black ink to the waveguide surface such that it extinguished the guided streak. If the white light was guiding in a waveguide mode, it would propagate in the waveguiding layer until it encountered the black spot, at which point it was extinguished. In contrast, the black ink had a negligible effect on white light propagating in substrate modes, simply because of the much smaller evanescent path length.

The visually observed waveguide response from the Xe lamp showed outcoupling of the entire visible spectrum over an incoupling arc of ~3°. The incoupling angle could be tuned over this 3° arc to achieve more efficient coupling for different wavelengths, with longer wavelengths guiding more efficiently at smaller angles (with respect to the prism surface normal). Raw throughput spectra for both TE and TM polarizations are shown in Figure 4. These spectra were acquired at the optimum incoupling angle for maximizing throughput in the 400-nm region, which decreased the throughput at >500 nm. It should be noted that these spectra can differ significantly among waveguides (vide infra). For the IOW used to acquire the data shown in Figure 4, the TE throughput was adequate to measure ATR spectra throughout the entire visible region. However, the poor TM throughput from 520 to 600 nm caused significant systematic errors in this spectral region due to stray light.
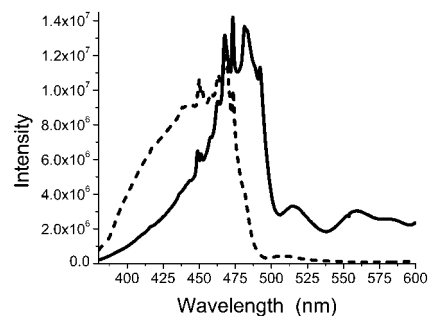
Figure 4. Raw spectral throughput of the broadband IOW spectrometer: TE polarized light (solid line) and TM polarized light (dashed line). The intensity measured is in arbitrary units registered by the CCD camera. The spectral response shown is for an incoupling angle optimized for maximum throughput at 400 nm (i.e., changing incident angle would significantly change the spectral throughput). Note the intense spikes in the region of maximum throughput that are due to intense source bands in this spectral region.

Waveguide Performance. The spectral performance of the broadband waveguide spectrometer was compared to that of a conventional UV−vis instrument (Spectral Instruments, model 440). This was accomplished by measuring transmission spectra of various narrow band-pass filters on both instruments. Instrument resolution was also assessed by measuring the fwhm of the various laser lines on both instruments.

Figure 5 shows a direct comparison of the transmittance of four narrow band-pass filters that span the visible spectrum. For the IOW spectrometer, the filters were placed in the beam path (Figure 1b), and the intensity propagated through the waveguide (I) was ratioed to the raw throughput spectrum (i.e., with no filter in the beam path, I_0). As Figure 5 shows, the response of the IOW spectrometer matches that of the commercial instrument very well, as evidenced by the nearly identical spectral profiles. A significant difference would indicate throughput problems in the wavelength region of the respective filter. The differences in peak maximum are most likely due to differences in wavelength calibration between the instruments. The approximate differences in peak position are: 2.2 (400-nm filter), 1 (514-nm filter), 0.9 (577-nm filter), and 1.5 nm (633-nm filter).

It is important to note that the ATR spectrum shown in Figure 5a demonstrates that the response of the broadband sol−gel IOW spectrometer extends down to at least 400 nm. This is a significant advance over previous designs, which were limited to performing measurements at wavelengths >500 nm. The data in Figure 5 show that the bandwidth is ~250 nm (390−645 nm), which is at least twice the bandwidth of previous broadband IOW spectrometers.[30−32]

The broadband response of an IOW is specific to a given waveguide in a particular coupling configuration and varies with waveguide parameters (e.g., waveguide layer thickness, uniformity, loss characteristics, etc.) and coupling conditions (e.g., coupling angle, intimacy of prism/waveguide contact, position of incident beam, etc.). The response can also vary for different polarizations. For example, the poor TM throughput in Figure 4 at >520 nm may be attributed to any one or a combination of these parameters. Although all of the sol−gel IOWs we have tested to date displayed broadband coupling, not all of them guided light over as broad a region as the IOW used to generate
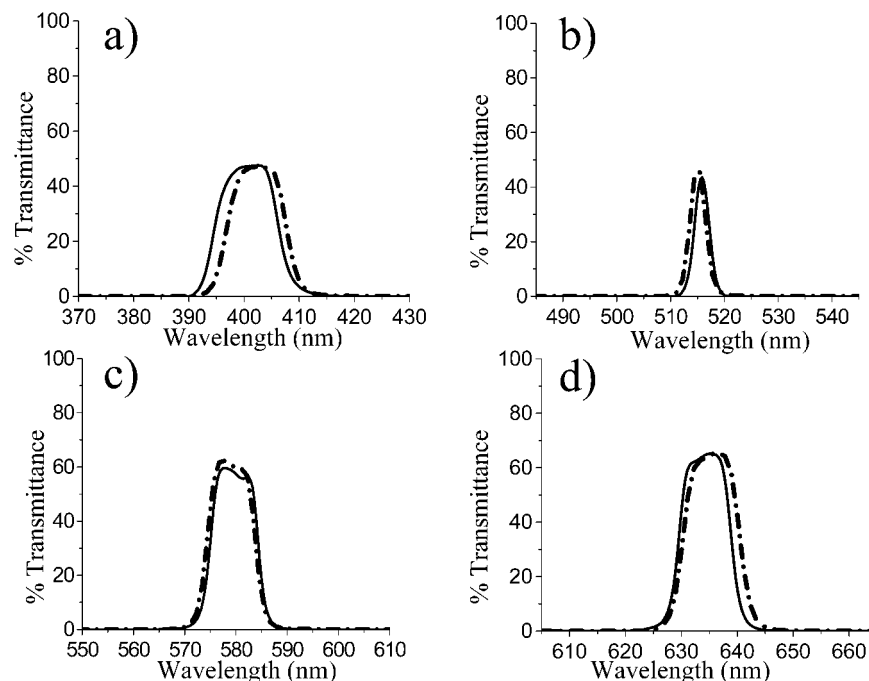
Figure 5. Spectral comparison between a broadband sol−gel IOW spectrometer and a conventional, transmission-based UV−vis spectrometer. The transmission spectra of four narrow band-pass filters that span the visible region of light are shown for both instruments (solid line = IOW, dashed line = conventional UV−vis). (a) 400-, (b) 514-, (c) 577-, and (d) 633-nm filters.
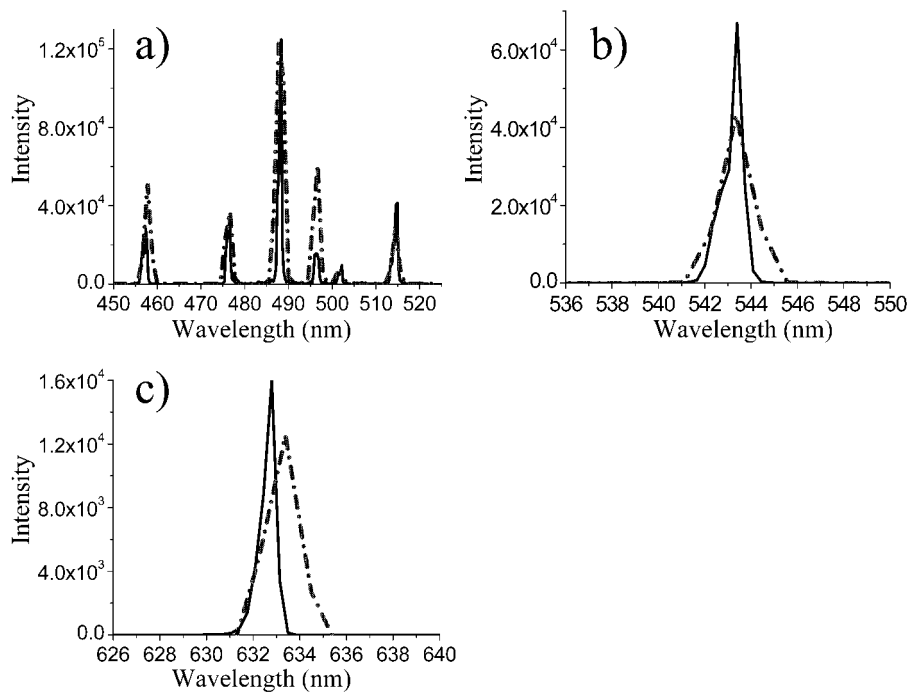
Figure 6. Resolution comparison between the broadband IOW spectrometer and a conventional transmission-based UV−vis spectrometer (solid line = IOW, dashed line = conventional UV−vis). The responses shown are for (a) Ar$^+$, (b) HeNe (543.4 nm), and (c) HeNe lasers (632.8 nm).

the data displayed in Figure 5. However, one of the benefits of the sol−gel waveguides employed here is simplicity. It is relatively easy to make large numbers of these waveguides having broadband responses that range from poor to excellent. Thus, even with moderate yields, multiple sol−gel waveguides with a desired broadband response can be fabricated in 1 day.

A comparison of resolution between the Spectral Instruments and the IOW spectrometers is shown in Figure 6. The resolution

was assessed by measuring the peak widths at half-maximum for multiple Ar$^+$ and HeNe laser lines. The conventional spectrometer uses fiber optics to deliver and collect light from a sample. Thus, the collection fiber was simply placed in the optical axis of the beam, with crossed polarizers used to attenuate the beam. Cross-examination of the data plotted in Figure 6 shows the laser line positions for the IOW and conventional instruments are all within 0.6 nm of their actual wavelengths. The fwhm of the laser lines

ranges from 0.5 to 1.3 nm for the broadband waveguide spectrometer and from 1.5 to 2.4 nm for the conventional transmission spectrometer. Thus, the fwhm values measured using the IOW spectrometer were narrower than those measured using the commercial instrument at all wavelengths. Overall, the data in Figures 5 and 6 clearly show that the response of the broadband IOW spectrometer is comparable to that of a commercially available transmission spectrometer currently used for conventional absorption spectrometry, demonstrating that the IOW apparatus is adequate for measuring molecular ATR spectra in the visible region.

The experimental limit of detection (LOD) for the IOW spectrometer was determined by measuring the spectral throughput multiple times in both TE and TM polarizations with the waveguide flow cell filled with sodium phosphate buffer. The mean and standard deviation of these blank intensity values (I_0) were then calculated at every wavelength. Since the LOD applies to measurements of very small absorbance values, it is reasonable to assume that the standard deviation of a sample intensity value (I) is approximately equal to the standard deviation of I_0. The standard deviations were propagated through absorbance = log-(I_0/I), and the limit of detection was taken to be three times the standard deviation of the absorbance. The mean of all LOD values from 400 to 600 nm was 8.0 milliabsorbance units (mAU) for TE polarization and 10.1 mAU for TM polarization. These relatively high LOD values can be attributed primarily to source fluctuation noise and could be improved by monitoring the intensities of the incident and transmitted beams simultaneously.[44]

Another important performance parameter determined for the broadband IOW spectrometer was the maximum measurable absorbance in the 400 nm spectral region for both TE and TM polarizations. Absorbance spectra of ferricytochrome c solutions of increasing concentration were measured in the same fashion as the band-pass filters described above (i.e., a cuvette containing solution was placed in the beam path at the filter stage). The blank for these measurements was a cuvette filled with buffer (data not shown). The stray light limit was then determined to be the point at which the Soret band absorbance reached a plateau, which was detected as a decreased ratio of absorbance values at the Soret band relative to the β band. The maximum measurable absorbances at 410 nm were 1.03 and 1.41 for TE and TM polarizations, respectively. Although these values were determined for the 400-nm region, they are also reasonable estimates of the maximum absorbance value measurable across the rest of the visible spectrum.

Protein Adsorption Experiments. Horse heart cytochrome c was chosen as a test sample for assessing the capabilities of the broadband sol−gel based IOW spectrometer for measuring ATR spectra of a submonolayer film. Cytochrome c was selected because (a) the absorbance of the Soret band near 410 nm is very strong, with molar absorptivities greater than 100 000 M^{-1} cm^{-1},

(40) Estabrook, R. W. *J. Biol. Chem.* **1957**, *223*, 781−794.
(41) Eaton, W. A.; Hochstrasser, R. M. *J. Chem. Phys.* **1967**, *46*, 2533−2539.
(42) Owens, J. W.; O'Connor, C. J.; Kassner, R. D. *Inorg. Chim. Acta* **1988**, *151*, 107−116.
(43) Coletta, M.; Costa, H.; De Sanctis, G.; Neri, F.; Smulevich, G.; Turner, D. L.; Santos, H. *J. Biol. Chem.* **1997**, *272*, 24800−24804.
(44) Bilhorn, R. B.; Epperson, P. M.; Sweedler, J. V.; Denton, M. B. *Appl. Spectrosc.* **1987**, *41*, 1125−1136.
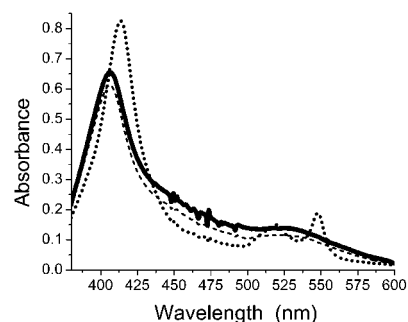
Figure 7. Absorbance spectra of a submonolayer of horse heart cytochrome c adsorbed to the surface of a sol−gel IOW, referenced to a phosphate buffer blank. The spectra were collected in the following order: (i) ferricytochrome c rinsed with a high-ionic-strength buffer (solid line), (ii) after the protein film was reduced with sodium dithionite (light dotted line), and (iii) after the film was reoxidized with ferricyanide (dark dashed line).

which allows for measurement of very small quantities of adsorbed material; (b) the protein adsorbs very strongly to hydrophilic glass, producing approximately monolayer coverage at dissolved concentrations of >10 μM. Initial experiments show that monolayer surface coverage produced spectra that were stray-light-limited in the Soret region. For this reason, after adsorption, the cytochrome c film was flushed with a high-ionic-strength buffer to desorb some of the adsorbed material and lower the measured absorbance in this region to <1 AU.

Figure 7 displays the ATR spectral response of an adsorbed submomolayer of horse heart cytochrome c. In this experiment, ferricytochrome c was adsorbed to the waveguide surface, the flow cell was flushed with a high-ionic-strength buffer, and then the spectra were collected both before and after the protein film was chemically reduced. Reduction caused a red shift of the Soret and β bands and the appearance of the α band, which is consistent with expectations based on the spectral properties of native (dissolved) cytochrome c.[45] The cytochrome c layer was then reoxidized, which caused a blue shift of the Soret and β bands and the disappearance of the α band. Note the signal reduction between the initial and reoxidized films, which is attributed to additional desorption of cytochrome c molecules during the course of the experiment. Note also the spikes near 450 nm in the initial ferricytochrome c spectrum, which are also apparent in Figure 4. These spikes are attributed to the xenon source and are difficult to quantitatively remove.

The spectral features of the adsorbed cytochrome c film shown in Figure 7 are qualitatively consistent with the features of native (dissolved) cytochrome c.[45] However, since the path length in a waveguide ATR geometry is wavelength-dependent, a correction must be applied before the ATR spectra can be quantitatively compared to the spectra of the native protein. A "waveguide path length correction" was, therefore, calculated and applied to the native spectra.

Derivation of the correction term begins with understanding the ATR spectral response. Quantitative ATR spectroscopy is based upon the well-known Beer−Lambert law,

(45) Margoliash, E.; Frohwirt, N. *Biochem. J.* **1959**, *71*, 570−572.

$$A = \epsilon bC \qquad (1)$$

where A is the absorbance, ϵ is the molar absorptivity, b is the internal reflection path length, and C is the concentration of the absorbing species. For waveguide ATR spectroscopy, the path length is defined for TE polarized light as[46]

$$b_{wg}{}^{TE} = h\left\{\frac{2n_l(n_w{}^2 - N_{TE}{}^2)L}{t_{eff,TE}N_{TE}(n_w{}^2 - n_c{}^2)}\right\} \qquad (2)$$

where h is the thickness of the light-absorbing film adsorbed to the waveguide surface, n_l is the refractive index of the adlayer, n_w is the refractive index of the waveguide layer, N_{TE} is the effective refractive index of the waveguide structure for TE polarized light, L is the distance between the incoupling element and the outcoupling element, n_c is the refractive index of the cover medium (superstrate), and $t_{eff,TE}$ is the effective thickness of the waveguide layer. The latter is given by

$$t_{eff,TE} = t + \frac{\lambda/2\pi}{(N_{TE}{}^2 - n_c{}^2)^{1/2}} + \frac{\lambda/2\pi}{(N_{TE}{}^2 - n_s{}^2)^{1/2}} \qquad (3)$$

where t is the waveguide layer thickness, λ is the wavelength of light, and n_s is the refractive index of the substrate on which the waveguide layer is supported. The expressions for TM polarized light are similar but contain several more terms. Since only TE polarized cytochrome c spectra are presented in this paper, the TM expressions are not given here, but are available in the literature.[46]

Equations 2 and 3 can be directly substituted into eq 1.

$$A = \epsilon\left(h\left\{\frac{2n_l(n_w{}^2 - N_{TE}{}^2)L}{t_{eff,TE}N_{TE}\ (n_w{}^2 - n_c{}^2)}\right\}\right)C \qquad (4)$$

Combining C with h allows eq 4 to be restated as

$$A = 1000\epsilon\sigma\left\{\frac{2n_l(n_w{}^2 - N_{TE}{}^2)L}{t_{eff,TE}N_{TE}(n_w{}^2 - n_c{}^2)}\right\} \qquad (5)$$

where σ is the surface coverage in moles/cm^2 (the 1000-fold scalar is necessary to convert liters to cm^3). This equation can be used to calculate IOW-ATR spectra from native spectra by substituting the native ϵ values, measuring various parameters of the waveguide structure in order to calculate the bracketed term, and assuming a surface coverage for the adsorbed film. It should be noted that eqs 2−5 were derived for a geometrically isotropic adlayer of chromophores. Similar relationships have been derived for geometrically anisotropic adlayers.[46]

Equation 5 was used to generate calculated IOW-ATR spectra to enable comparison with the experimental spectra. The ϵ values used for native oxidized and reduced horse heart cytochrome c were those reported by Margoliash and Frohwirt.[45] Values for σ were assumed (vide infra), n_w and t were experimentally deter-

(46) Mendes, S. B.; Saavedra, S. S. *Appl. Opt.* **2000**, *39*, 612−621.
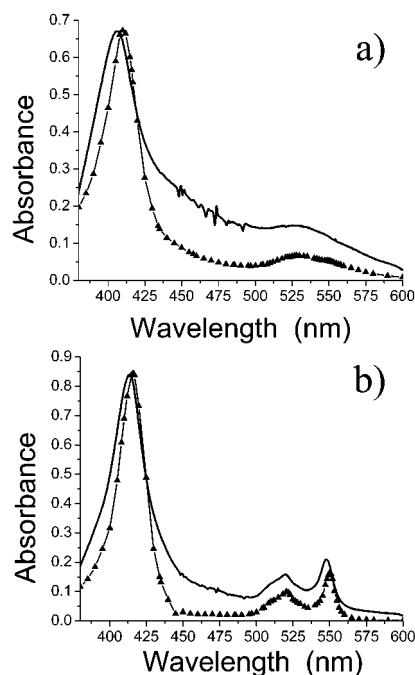
Figure 8. Experimental IOW-ATR spectra of a submonolayer film (solid lines) of (a) ferricytochrome c and (b) ferrocytochrome c. Calculated IOW-ATR spectra (▲) of (a) native ferricytochrome c and (b) native ferrocytochrome c.

mined[37] (vide supra), and L was measured. The effective refractive index was calculated from the relation $N_{TE} = n_w \sin\theta_w$, where the internal waveguide angle (θ_w) is calculated from the external incident angle using Snell's law. The optical dispersion curve for n_c was generated from tabulated values,[47] and a value of 1.51 was used for n_s. Finally, the quantity n_l was assumed to be equal to n_c.[46]

Figure 8a shows a comparison between the calculated and experimental spectra of ferricytochrome c. The surface coverage chosen for the calculation was 9.75×10^{-13} mol/cm^2, which corresponds to 4.9% of a close-packed monolayer.[16] This value was selected to produce an absorbance value similar in magnitude to the experimental absorbance at 410 nm (i.e., the oxidized Soret band maximum). Likewise, Figure 8b is a comparison between the calculated and the experimental spectra of ferrocytochrome c. In this case, the surface coverage was chosen to be 1.0×10^{-12} mol/cm^2, which corresponds to 5.0% of a full monolayer. Again, σ was chosen to match the experimental absorbance at the Soret band maximum at 416 nm.

Comparison of the experimental and calculated spectra in Figure 8 reveals a small wavelength offset. This is likely due to an error in wavelength calibration, as observed in the spectra of the band-pass filters (Figure 4). With respect to band shape, it is apparent that the spectra of the adsorbed protein film contain the spectral features of native cytochrome c. However, there are some significant differences. The thin-film spectra display higher absorbance values than the calculated spectra at most wavelengths. Furthermore, the Soret bands are broader in the experimental spectra. At this point, it is important to emphasize that by displaying the data as shown in Figure 8, we have made the

(47) Thormaehlen, I.; Straub, J.; Grigull, U. *J. Phys. Chem. Ref. Data* **1985**, *14*, 933−945.

assumption that the molar absorptivities of adsorbed cytochrome *c* and native cytochrome *c* are equal. However, it is well-known that adsorption at a solid−liquid interface may induce changes in native conformation of a protein.[48] Furthermore, if the surface of the adsorbent is chemically heterogeneous, then a distribution of adsorbed protein conformations will likely result. Thus, the differences in band shape between the experimental and calculated spectra apparent in Figure 8 may be due to adsorption-induced conformational changes that alter the photophysical properties of the heme moieties in the protein film. However, more extensive studies will be required to systematically address this hypothesis.

Finally, the relative sensitivity of the broadband IOW spectrometer for measuring ATR spectra of thin films can be assessed by predicting the absorbance that would be measured in a conventional transmission format. By combining path length *b* with concentration *C*, which gives surface coverage σ, and recasting ϵ in units of cm^2/mol, eq 1 can be used to calculate the absorbance of a transmission measurement of a cytochrome *c* film. The calculated absorbance for the Soret band of a ferricytochrome *c* film with a surface coverage of 9.75×10^{-13} mol/cm^2 is 1.03×10^{-4} AU ($\epsilon_{410\ nm} = 106\ 100$ M^{-1} cm^{-1}). Thus, the IOW-ATR spectrometer provides a sensitivity advantage of $\sim 10^4$ relative to a conventional transmission geometry.

(48) See, for example: (a) Brash, J. L.; Horbett, T. A. in *Proteins at Interfaces II*; Horbett, T. A., Brash, J. L., Eds.; ACS Symposium Series 602; American Chemical Society: Washington DC, 1995; pp 1−23, and references therein. (b) Hlady, V.; Buijs, J. *Curr. Opin. Biotechnol.* **1996**, *7*, 72−77, and references therein.

CONCLUSIONS

We have constructed a broadband, planar IOW-ATR spectrometer based on a simplified incoupling arrangement, relative to previous designs. The performance of this spectrometer compares well with that of a commercially available, transmission-based instrument. The capability of this device to measure broadband ATR spectra of thin molecular films over the entire visible wavelength range (390 nm to at least 645 nm) is unprecedented for a single-mode IOW platform. As opposed to previous broadband designs, the sol−gel waveguide can be aggressively cleaned with oxidizing acids and reused multiple times. Although not shown here, the spectrometer can be used to collect both TE and TM polarized spectra of waveguide-supported molecular films. The ability to measure polarized ATR spectra make this spectrometer a useful research tool for studying molecular orientation in thin films.